
Magnetisation, excitation and relaxation

AT A FUNDAMENTAL level, the NMR effect is reliant on spin, a phenomenon which, on the scale of individual nuclei, is firmly in the realm of quantum mechanics. Population differences in spin state amongst a very large number of these nuclei give rise to a residual magnetisation, which in turn is the reason that we can retrieve a signal during an MRI scan. By adding energy to a stable system of spins, we can provoke a change in the magnetisation pattern of the system, which can be measured as the spins relax back to their resting states. Moreover, by applying sequences of excitations to brain tissue, and fine-tuning the relaxation process, images of the tissue can be recovered. This chapter provides a basic grounding in these processes, to support the material that follows in later chapters.

3.1 State and spin

For a simple Newtonian system such as a moving ball, the dynamical state of the system consists of such quantities as position and momentum, which can in principle be established exactly, and which describe the instantaneous behaviour of the ball with certainty. In a quantum mechanical system, on the other hand, dynamical variables such as position do not have well-defined values at any given time; instead, quantum mechanical theory describes probability distributions over these variables. A measurement of position, for example, is therefore a nondeterministic experiment; and until such a measurement is made, the state of any single quantum object is uncertain.

A form of notation introduced by Paul Dirac allows us to discuss quantum state in abstract terms without concerning ourselves with the details of the particular system we are working with. Using this *bra-ket notation*, quantum state can be described and manipulated using the familiar principles of linear algebra (Dirac, 1958). Full details of the underlying physics, as well as a far more detailed general introduction to quantum mechanics than the sketch which follows, can be found in Bransden & Joachain (1989).

Under Dirac's system, the instantaneous state of a quantum mechanical system is represented by a vector in some state space over the complex numbers, whose dimensionality depends on the characteristics of state in which we are interested. These vector elements of the state space are known as ket vectors, or **kets**, and are written using the notation $|\cdot\rangle$, where the dot is to be replaced by a label. The formulation is such that the direction of these vectors is the only property that distinguishes one state from another; lengths are immaterial, and so generally normalised. Consequently, $|\psi\rangle = c|\psi\rangle$ for any nonzero complex scalar, c . On the other hand, some combination

$$|x\rangle = x_1|\psi_1\rangle + x_2|\psi_2\rangle$$

is, in general, different to each of the states $|\psi_1\rangle$ and $|\psi_2\rangle$. In fact, the composite ket, $|x\rangle$, represents a *superposition* of the two constituent states. The significance of this will be explained

shortly.

If we assume that some set of ket vectors, $\{|\psi_i\rangle\}$, forms a basis for the state space we are interested in, then any arbitrary ket can be represented as some linear combination of the set, whose coefficients form a column vector (i.e. single-column matrix):

$$|x\rangle = \sum_{i=1}^n x_i |\psi_i\rangle = \begin{bmatrix} x_1 \\ x_2 \\ \vdots \\ x_n \end{bmatrix} \Psi. \quad (3.1)$$

The matrix Ψ represents the whole basis set. We note briefly that every ket has a corresponding *bra*, denoted $\langle \cdot |$, which is formed by taking the adjoint of the ket vector, which is the combined operation of matrix transposition and complex conjugation. Thus, a bra in matrix representation is a row vector whose coefficients are the complex conjugates of the elements of the ket. That is,

$$\langle x| = |x\rangle^\dagger = \Psi^\dagger \begin{bmatrix} x_1^* & x_2^* & \dots & x_n^* \end{bmatrix},$$

where † represents the adjoint, and $*$ the conjugate. By multiplying together a bra and a ket, we obtain

$$\langle x|y\rangle = \sum_{i=1}^n x_i^* y_i \langle \psi_i | \psi_i \rangle,$$

which simplifies to

$$\langle x|y\rangle = \sum_{i=1}^n x_i^* y_i \quad (3.2)$$

because the basis kets, like all state kets, are normalised to unit length. Eq. (3.2) is exactly the form of the inner product between $|x\rangle$ and $|y\rangle$.

That quantum state spaces are complex-valued is significant. Recall that the complex number $z = a + ib$ can be written in an alternative polar form, $z = re^{i\theta}$, such that

$$a = r \cos \theta \quad b = r \sin \theta \quad r = |z| = \sqrt{a^2 + b^2}$$

and i is the imaginary unit, with $i^2 = -1$. The complex conjugate is then given by

$$z^* = a - ib = re^{-i\theta}.$$

In polar form, r is sometimes referred to as the amplitude, and θ as the phase. It is precisely the fact that quantum theory allows for phase effects which enables it to explain results such as Claus Jönsson's double slit electron diffraction experiment, which demonstrated wavelike behaviour in particles just as Thomas Young had done for light more than a century and a half before (Jönsson, 1974).

It might be expected in such a system as this, where vector length has no physical implication for the state represented by a particular ket, that eigenvectors are of significant importance; and indeed they are central to quantum physics. Physical properties of quantum systems, such as momentum or position, are associated with linear operators in the Dirac formalism. In particular, these so-called *observable* operators are self-adjoint, so that $A^\dagger = A$; and as such their eigenvectors are orthogonal and their eigenvalues are always real (Riley *et al.*, 2002, §8.13.2). As a result the *eigenstates*, $|\varepsilon\rangle$, which satisfy

$$A|\varepsilon\rangle = \lambda|\varepsilon\rangle$$

for real scalar values of λ , make up a natural orthonormal basis set for the state space in which the observable A operates.

One such observable property is **spin**, a quantum characteristic which is intrinsic to particles such as protons and has no classical equivalent. These particles can be thought of as having a natural angular momentum which causes them to spontaneously spin in place. Consider a

single component of this three-dimensional spin, along a direction which we will choose to be the z axis of some physical space—in the case of protons, which are abundant in brain tissue, the corresponding spin operator, S_z , has two eigenstates, which are called “spin up” and “spin down” and may be thought of as analogous to clockwise and anticlockwise. The *magnetic quantum number* of the proton, m , takes the value $\frac{1}{2}$ for the spin up state, and $-\frac{1}{2}$ for the spin down. Since the eigenstates are orthonormal, the inner product of any pair of them is given by the Kronecker delta. That is,

$$\langle m|m'\rangle = \delta_{mm'} = \begin{cases} 1 & \text{for } m = m' \\ 0 & \text{for } m \neq m' . \end{cases} \quad (3.3)$$

As described in Eq. (3.1), an arbitrary spin state, $|\psi\rangle$, can then be described as a linear combination of the spin up and spin down eigenstates:

$$|\psi\rangle = \sum_m p_m |m\rangle .$$

In these circumstances, where the basis vectors are a set of eigenstates, the coefficients, p_m , are called *probability amplitudes*, and have a specific practical significance: their squared moduli represent the probability masses associated with each basis vector in the state $|\psi\rangle$. This probability mass function associated with the state of the system manifests itself when the state is measured, such that

$$\Pr(M = m) = |p_m|^2 = p_m^* p_m , \quad (3.4)$$

where M is the random variable representing the measured spin value.^a It is important to remember that a measurement of the spin of a proton can *only* yield one of the two values $\pm\frac{1}{2}$, which make up the discrete sample space of M .

Given this interpretation of the superposed state, we can immediately write down the expected value of a spin measurement by referring back to Eq. (2.9). It is

$$\langle M \rangle = \sum_m m P(m) = \sum_m |p_m|^2 m . \quad (3.5)$$

The orthonormality of the eigenstates described by Eq. (3.3) allows us to expand this as

$$\sum_m \sum_{m'} p_m^* p_{m'} m \langle m|m'\rangle ,$$

which can be expanded in matrix form—provided that S_z is correctly constructed—to $\langle \psi|S_z|\psi\rangle$, a full *bracket*, which is the way that expectation values are written in Dirac notation. Given an obvious formulation of orthonormal eigenstates in this two-dimensional state space, viz.

$$\left| \frac{1}{2} \right\rangle \text{ or } |\uparrow\rangle = \begin{bmatrix} 1 \\ 0 \end{bmatrix} \quad \left| -\frac{1}{2} \right\rangle \text{ or } |\downarrow\rangle = \begin{bmatrix} 0 \\ 1 \end{bmatrix} ,$$

this formulation works out correctly if we take as the spin operator

$$S_z = \frac{1}{2} \begin{bmatrix} 1 & 0 \\ 0 & -1 \end{bmatrix} , \quad (3.6)$$

which has no off-diagonal components and is therefore trivially self-adjoint.

^aThe process of measurement is a crucial and counterintuitively complex one in quantum mechanics. The question of what constitutes a measurement is a controversial one, but the essential outcome is a sampling from the distribution given by Eq. (3.4), and an apparent “collapse” of the system’s state into the eigenstate corresponding to the outcome, so that repeated measurements will all produce this same outcome.

3.2 Protons in a magnetic field

It is unlikely to come as a surprise that quantum state is not a time-invariant phenomenon. The observable that determines the evolution over time for a quantum mechanical system is energy, which is represented mathematically by a *Hamiltonian* operator, H . Given the appropriate Hamiltonian, the change in state of the system is described in general by the famous time-dependent *Schrödinger equation*. In the special case where the Hamiltonian itself has no time dependence, the general equation can be separated into two: the time-independent Schrödinger equation, which takes the form of an eigenvalue equation; and a relationship describing the time evolution of the system (Bransden & Joachain, 1989). Specifically, we get

$$H|\psi(t)\rangle = E|\psi(t)\rangle \quad (3.7)$$

and

$$H|\psi(t)\rangle = i\hbar \frac{\partial}{\partial t} |\psi(t)\rangle, \quad (3.8)$$

where \hbar is the reduced Planck constant, which corresponds to the size of a fundamental quantum of energy. Integrating Eq. (3.8) leads directly to the solution

$$|\psi(t)\rangle = \exp\left(\frac{-iHt}{\hbar}\right) |\psi(0)\rangle. \quad (3.9)$$

Now, we may note that if $|\psi(0)\rangle$ is an eigenstate of the Hamiltonian with eigenvalue E —as per Eq. (3.7)—then H will be replaced by E in this solution, and the time evolution of the system will amount to a mere multiplication of the eigenstate by a complex constant; which, as we know, has no effect on the physical state of the system. Consequently, a system that is in a state that is an eigenstate of the Hamiltonian will stay in that state, unless some external influence dislodges it.

Nuclei with spin, such as that of hydrogen (^1H , which contains just a single proton), act like tiny magnets. If all three components of the spin of a proton are represented by \mathbf{S} , then it will have a magnetic dipole moment of $\boldsymbol{\mu} = \gamma\hbar\mathbf{S}$, where γ is called the **gyromagnetic ratio**, which varies from one species of nucleus to another. As a result of this dipole moment, an external magnetic field will have a significant effect on these nuclei. The Hamiltonian corresponding to the interaction with a static magnetic field applied in the z direction is given by

$$H = -\gamma\hbar B_0 S_z, \quad (3.10)$$

where B_0 is the field strength (Callaghan, 1991). By substituting Eq. (3.10) into Eq. (3.7) and rearranging, we obtain

$$S_z |\psi(t)\rangle = -\left(\frac{E}{\gamma\hbar B_0}\right) |\psi(t)\rangle,$$

which is an eigenvalue equation for S_z . However, we already know that the eigenvalues of this operator are $\pm\frac{1}{2}$, so we can obtain immediately

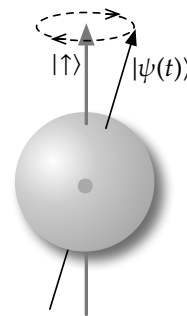
$$-\left(\frac{E}{\gamma\hbar B_0}\right) = \pm\frac{1}{2};$$

and so

$$E = \mp \frac{\gamma\hbar B_0}{2}. \quad (3.11)$$

Notice the signs: the energy of the spin up state is lower than that of the spin down state. It is clear from Eq. (3.11) that the separation between the energy levels corresponding to the two possible values of m is given by $\Delta E = \gamma\hbar B_0$. This difference is called the *Zeeman splitting*, and gives the magnitude of the energy quantum needed to excite a transition from one Zeeman state to the other. The de Broglie relation, $\Delta E = \hbar\omega$, tells us that a photon with angular frequency $\omega = \gamma B_0$ —the so-called **Larmor frequency**—would be able to supply the required energy.

Figure 3.1: A spin state that is not an eigenstate will undergo spontaneous precession about the spin up direction, thereby tracing out the pathway indicated here by a dashed line.



We can also consider the time evolution of this system by substituting Eq. (3.10) into Eq. (3.9), which gives

$$|\psi(t)\rangle = \exp(i\gamma B_0 \mathbf{S}_z t) |\psi(0)\rangle. \quad (3.12)$$

The time evolution operator in equation Eq. (3.12)—the exponential term—represents a phase rotation of the state about the z axis by an angle $\gamma B_0 t$. Hence, all noneigenstates will precess about the z axis (i.e. the direction of B_0) at the Larmor frequency. This is illustrated in Fig. 3.1.

As a result of the difference in energy between the two eigenstates, the p.m.f. over spin states for any given proton is not uniform at thermal equilibrium. Rather, a large population of spins will be distributed amongst the Zeeman energy levels according to the Boltzmann distribution, viz.

$$n_{\downarrow}/n_{\uparrow} = \exp(-\Delta E/kT) = \exp(-\gamma \hbar B_0/kT), \quad (3.13)$$

where n_{\uparrow} and n_{\downarrow} are the number of spins parallel and antiparallel to the magnetic field respectively, k is Boltzmann's constant, and T is the absolute temperature. However, in a 1.0 T field and at normal body temperature (310 K), the fractional excess of protons in the low energy state, $(n_{\uparrow} - n_{\downarrow})/(n_{\uparrow} + n_{\downarrow})$, is only 3.295×10^{-6} . Nevertheless, this small difference is significant, and in a large population of spins within a some small region of space—known as an *isochromat*—it is large enough to be measurable on a macroscopic scale.

The **magnetisation** of an isochromat at equilibrium, containing a net excess of N spins in the positive z direction, is defined as $\mathbf{M}_0 = N\boldsymbol{\mu}$, where $\boldsymbol{\mu}$ is the proton magnetic moment discussed above. It follows from Eq. (3.13), therefore, that the magnitude of this vector is approximately given by

$$M_0 = \chi B_0 \simeq \frac{\gamma^2 \hbar^2 B_0 (n_{\uparrow} + n_{\downarrow})}{4kT}. \quad (3.14)$$

The factor χ , which links the magnetisation of the isochromat with the static field strength, is called its *magnetic susceptibility*.

It is clear from Eq. (3.14) that the magnetisation can be increased for a fixed group of spins, thereby increasing sensitivity, by increasing the field strength or decreasing the temperature. However, since the change would have to be substantial to make any significant difference, the latter option is not very practical for *in vivo* MRI!

At rest, the direction of the magnetisation vector, \mathbf{M}_0 , is the same as that of the static field. However, in a nonequilibrium state, this vector could have any arbitrary direction. Whilst the underlying spins must always yield one or other of the eigenstates when measured, the semiclassical representation of spin dipole moments as magnetisation is approximately continuous, since it denotes the aggregate tendency of a large number of individual quantised states.

3.3 The NMR signal

As we have seen, a nucleus with spin can be excited from the spin up to the spin down state using electromagnetic radiation with an angular frequency corresponding to the appropriate Larmor frequency. For ^1H nuclei, this corresponds to a linear frequency of about 42.5 MHz T^{-1} , which is in the radiofrequency (RF) range.

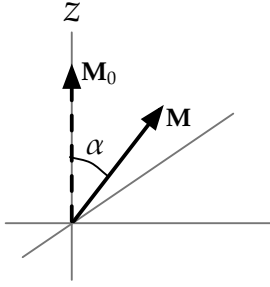


Figure 3.2: The effect of applying a radiofrequency electromagnetic pulse to a spin isochromat at equilibrium is to “flip” the magnetisation vector, \mathbf{M} , by an angle α towards the transverse (x - y) plane.

If a spin isochromat is excited so that half of the “excess” protons—which are responsible for the residual magnetisation at equilibrium—are expected to be in each of the spin up and spin down states, then clearly no magnetisation in the longitudinal (z) direction remains, because there is no longer any net difference between the populations of spins in each state. However, since the states of the spins are individually precessing about the z axis, as shown in Fig. 3.1, a net magnetisation in the transverse (x - y) plane can arise if the spins are in phase with one another, due to constructive interference. This is exactly the effect of applying an RF pulse to an isochromat at equilibrium (see Fig. 3.2). Since the initial magnetisation vector, \mathbf{M}_0 , does not precess, the spins will be in phase after the excitation has “flipped” the magnetisation towards the transverse plane. The exact angle, α , by which the magnetisation vector is deflected will depend on the power of the RF pulse and the length of time over which it is applied; but these parameters can be calibrated so as to produce predictably any flip angle required.

The evolution over time of the components of the magnetisation vector due to precession is given by

$$\frac{d\mathbf{M}}{dt} = \gamma \mathbf{M} \wedge \mathbf{B}, \quad (3.15)$$

where \wedge is the vector cross product, and \mathbf{B} is the total magnetic field. The latter primarily consists of the static field, \mathbf{B}_0 , but the RF pulse also induces a small and fluctuating field, \mathbf{B}_1 , perpendicular to the longitudinal direction.

Eq. (3.15) does not, however, represent the whole picture. An excited isochromat will not merely precess indefinitely at a fixed angle from the longitudinal direction; rather, its magnetisation will gradually return to the equilibrium state. This relaxation is caused by a combination of processes. Firstly, some of the excitation energy will be spontaneously transferred to the environment as heat—an exponential decay process known as spin-lattice relaxation. Evolution of the z component of the magnetisation is therefore more accurately reflected by

$$\frac{dM_z}{dt} = \gamma(M_x B_y - M_y B_x) - \frac{M_z - M_0}{T_1}, \quad (3.16)$$

where T_1 is a time constant. The second relaxation process involves the transfer of energy between excited spins, which causes their rates of precession to vary slightly from one to the other. This in turn results in a dephasing of the spin states, so that the transverse component of the magnetisation vector diminishes; again exponentially:

$$\frac{dM_x}{dt} = \gamma(M_y B_z - M_z B_y) - \frac{M_x}{T_2} \quad \frac{dM_y}{dt} = \gamma(M_z B_x - M_x B_z) - \frac{M_y}{T_2}. \quad (3.17)$$

This second time constant T_2 is, in general, not equal to T_1 ; but it cannot be larger. Eqs (3.16) and (3.17) are collectively the *Bloch equations* for nuclear induction (Bloch, 1946).

Once the RF pulse has been applied to excite the system it is switched off, leaving the z component of \mathbf{B} as the only nonzero one (the static field is still on). Under these conditions we can therefore ignore all terms in the Bloch equations containing B_x or B_y . The resulting

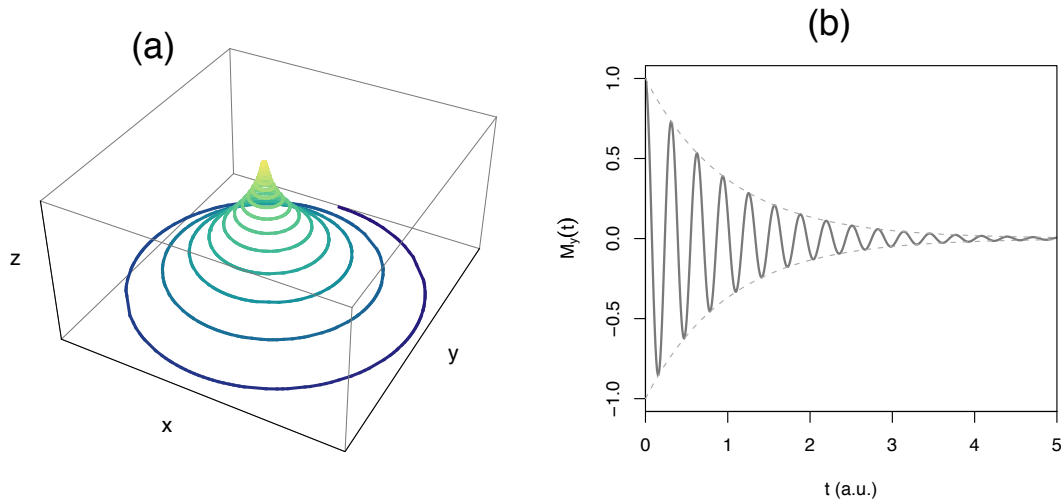


Figure 3.3: Effects of relaxation on the magnetisation vector after a 90° excitation pulse. **(a)** The vector precesses around the z axis with a monotonically decreasing radius. **(b)** The y component of the relaxing magnetisation vector (or equivalently, the x component) induces a decaying voltage in the receive coil. In both subfigures, $T_1 = 2T_2$.

simplified differential equations can be integrated to give the solutions

$$\left. \begin{aligned} M_x(t) &= (c_1 \cos(\gamma B_z t) + c_2 \sin(\gamma B_z t)) e^{-t/T_2} \\ M_y(t) &= (c_2 \cos(\gamma B_z t) - c_1 \sin(\gamma B_z t)) e^{-t/T_2} \\ M_z(t) &= M_0 + c_3 e^{-t/T_1} \end{aligned} \right\}, \quad (3.18)$$

where c_1 , c_2 and c_3 are constants; although there is no loss of generality in taking $c_1 = 0$, so we will do so. The x and y components of the magnetisation will then trace out a circle of radius $c_2 e^{-t/T_2}$ with angular frequency γB_z , which is the Larmor frequency for the main field. This radius is itself dependent on time, clearly, and will monotonically decrease as relaxation proceeds; as shown in Fig. 3.3(a).

If an electrically conducting coil is placed around the subject in the transverse plane, the rotating transverse magnetisation component will induce a voltage in it—just as in an electrical generator—whose magnitude will decay exponentially due to relaxation (see Fig. 3.3(b)). It is this phenomenon, known as a **free induction decay** (FID), which forms the signal for an NMR experiment. Note that M_x and M_y differ only in phase, and they make up the real and imaginary components of the complex-valued oscillating function $M_{xy}(t) = c_2 e^{-t/T_2} e^{i\omega t}$, where $\omega = \gamma B_z$ above. It is often convenient to work with the transverse magnetisation in these terms.

3.4 Pulse sequences

The relaxation time constants, T_1 and T_2 , are not invariant throughout the brain; or, indeed, the body (de Certaines *et al.*, 1993). Moreover, there can be systematic differences in these parameters between healthy and pathological tissue of the same basic type. It is therefore constructive from a clinical point of view to devise NMR-based protocols for measuring rates of relaxation; or at least, for creating contrast between regions whose rates differ. This aim can be achieved by applying carefully designed sequences of RF pulses to brain tissue.

A simple pulse sequence for weighting the signal by the value of T_1 is called inversion recovery. At its simplest, this sequence consists of a pulse inducing a flip angle of 180° ,

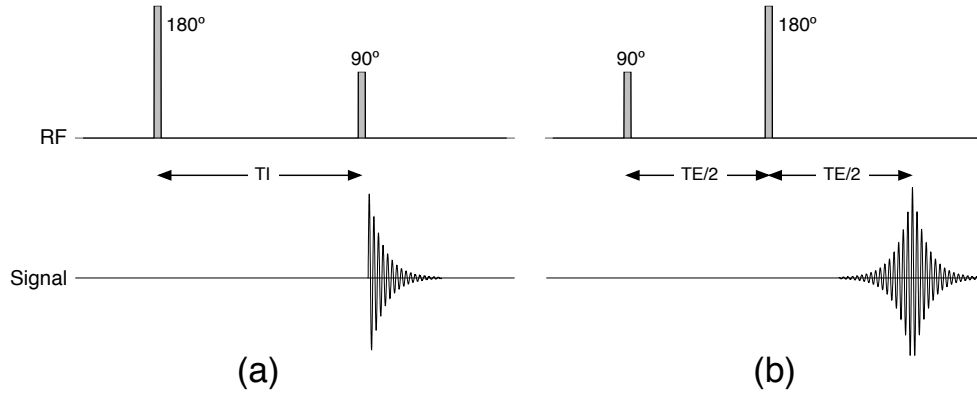


Figure 3.4: Pulse sequence timing diagrams for inversion recovery (a) and spin-echo (b) sequences. The axis represents time, but pulse and signal widths are not to scale.

followed after a time τ_1 by a 90° pulse. The first of these—the inversion pulse—will flip an isochromat at equilibrium so that all of the magnetisation is antiparallel to the static field. The system will then decay back towards the equilibrium state according to

$$M_z(t) = M_0 \left(1 - 2e^{-t/T_1}\right), \quad (3.19)$$

until the second pulse is applied to convert the remaining longitudinal magnetisation into measurable transverse magnetisation. Note that Eq. (3.19) is a special case of Eq. (3.18) in which $c_3 = -2M_0$, the choice that produces the correct boundary conditions. By measuring the FID amplitude for several values of the inversion time, τ_1 , one can infer the value of T_1 in a sample.

The same pair of pulses in the opposite order can be used to give T_2 -weighting, in a technique known as spin-echo (Hahn, 1950). The spins are allowed to dephase for a time $T_E/2$, after which the magnetisation is flipped. After another time period of $T_E/2$ the spins, which are now dephasing in the opposite sense, will return to being in phase with one another, thus producing a measurable signal. Once again, the constant T_2 can be recovered by repeating the experiment with several values of the echo time, T_E . A significant benefit of this approach is that the separate dephasing effects of small local variations in the main static field—which are always present to some degree—will cancel out at the time the FID amplitude is measured.^b The transverse magnetisation component will therefore evolve according to

$$M_{xy}(t) = M_0 e^{-t/T_2} e^{i\omega t}, \quad (3.20)$$

a version of Eq. (3.18) with $c_2 = M_0$. This is valid as long as *all* of the equilibrium magnetisation is initially flipped into the transverse plane. In order to ensure that this is the case, the repetition time, τ_R , between successive 90° pulses in a train of spin-echoes must be sufficiently large to allow the longitudinal magnetisation to recover fully.

The inversion recovery and spin-echo pulse sequences are illustrated in Fig. 3.4, in a schematic representation called a *pulse sequence timing diagram*.

In order to make the move from NMR to MRI, we need the ability to localise a signal in space. Spatial information can be encoded in the signal by applying magnetic *gradients*—that is, static magnetic fields whose strength varies (linearly) across a region of space. The magnitude of these gradients is small compared to that of the main field—typically on the order of 10^{-2} T m^{-1} —but they are large enough to provoke variation in the angular frequency at which local magnetisation vectors precess. A gradient with magnitude and orientation described by

^bIn fact, this is only true under the (naïve) assumption that spins do not move during the experiment. In practice, there is movement within the field between the 90° pulse and the signal measurement; a fact which is exploited by diffusion MRI, as we will see in chapter 4.

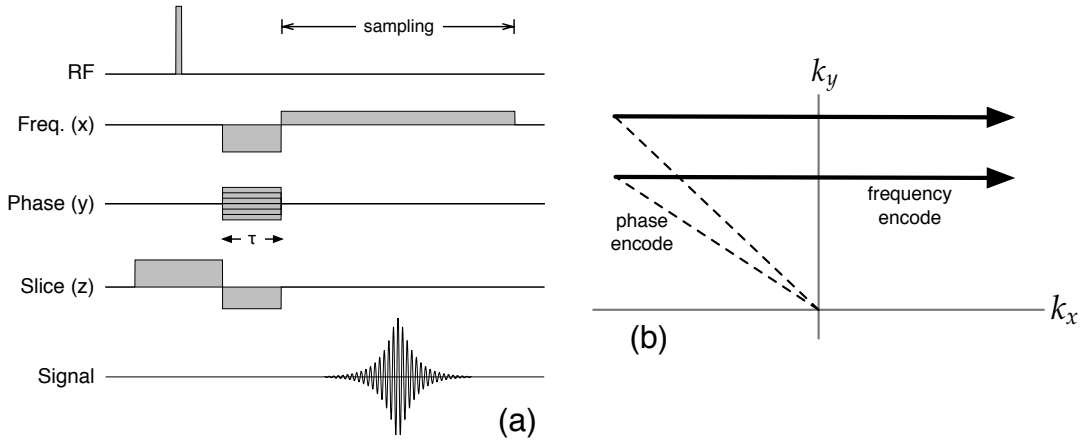


Figure 3.5: The spin-warp imaging sequence. A phase encoding gradient is applied, typically along the y axis, for a time τ ; after which a frequency encoding gradient is applied along the x axis, and the FID signal is sampled. This process is repeated a number of times with different magnitudes of phase encoding to build up a full three-dimensional brain volume. The sequence is shown as a pulse sequence timing diagram (a) and in terms of its characteristic trajectory in \mathbf{k} -space (b).

a vector $\mathbf{G} = (G_x, G_y, G_z)$ will produce a local frequency shift, relative to the Larmor frequency, described by

$$\omega(\mathbf{r}) = \gamma \mathbf{G} \cdot \mathbf{r} = \gamma(G_x r_x + G_y r_y + G_z r_z),$$

where $\mathbf{r} = (r_x, r_y, r_z)$ represents location in the brain. After applying a 90° RF pulse to create a measurable FID, the signal from a small volume of tissue is therefore given by

$$dA(\mathbf{G}, t) = \rho(\mathbf{r}) \exp(i\gamma t \mathbf{G} \cdot \mathbf{r}) d\mathbf{r}. \quad (3.21)$$

We ignore the effects of spin-spin (T_2) relaxation for simplicity, but in a real experiment its effect needs to be quantified. Morris (1986) provides a detailed explanation of the impact it has on the signal. The scalar field $\rho(\mathbf{r})$ represents the number of spins per unit volume at each location in the brain. This spin density is proportional to the initial magnetisation, M_0 , as we saw in Eq. (3.14); and it is this property that we wish to recover in our experiment. The signal value denoted by the left hand side of Eq. (3.21) is therefore not exactly the FID described by the Bloch equations, but it is closely related to it. Now, introducing

$$\mathbf{k} = \frac{1}{2\pi} \gamma \mathbf{G} t,$$

the signal over the whole brain is given by integrating Eq. (3.21):

$$A(\mathbf{k}) = \int \rho(\mathbf{r}) \exp(i2\pi \mathbf{k} \cdot \mathbf{r}) d\mathbf{r}. \quad (3.22)$$

Eq. (3.22) describes a Fourier relationship between the spin density throughout the brain, $\rho(\mathbf{r})$, and the measured signal in the presence of magnetic gradients; and it is therefore the fundamental relationship in MRI. If we sample the signal at a number of locations in \mathbf{k} -space, we can recover the spin density using a discrete Fourier transform.

There are a number of schemes for traversing \mathbf{k} -space with various advantages and disadvantages, but we will just describe a relatively straightforward one to give the idea. Fig. 3.5 shows a sequence called spin-warp (Edelstein *et al.*, 1980). It should be noted that this is an imaging sequence using gradients, which is quite independent from the sequences of RF pulses which are used to affect contrast.

The timing diagram in Fig. 3.5(a) shows that after the RF pulse is applied, a gradient is applied for a certain time, τ , along the y axis. The effect is to apply a phase offset to the

magnetisation vectors, $\gamma\tau G_y r_y$, which depends on their position in the y direction—thereby encoding position information in the phase of the signal. Immediately afterwards, another gradient is applied in the x direction, and is maintained while the signal is sampled. In this case, the frequency of precession of the magnetisation vectors as time progresses is altered by an amount $\gamma G_x r_x$ —as we saw above—which depends on the location of the tissue along the x axis. This combination of frequency and phase encoding allows one to spatially locate the source of parts of the signal within a two-dimensional plane. Localisation in the third dimension of space is achieved by selective excitation: that is, only a single “slice” of a certain thickness is excited at a time, and the 3-D image is then built up from a series of these 2-D slices.^c A slice selection gradient is applied at the same time as the RF pulse.

As a trajectory through \mathbf{k} -space, the sequence is easily represented. Fig. 3.5(b) shows it in these terms. The phase encode step, along with the application of a negative gradient in the frequency encode direction at the same time, moves us to the “leftmost” position in the space for some value of k_y . Then, during the application of the frequency encoding gradient, the trajectory moves in the positive x direction, and all the signal data for this phase encode level is recorded. This process is repeated for several different magnitudes of phase encode gradient, and \mathbf{k} -space is thereby sampled line-by-line.

The spin-warp sequence requires a separate RF pulse for each line of \mathbf{k} -space, which limits the rate at which images can be acquired. On the other hand, an influential alternative technique called echo-planar imaging (EPI) is able to reconstruct an entire 2-D slice image using a single excitation pulse or “shot” (Mansfield, 1977). This method is now widely used because of its speed advantages, especially in studies that require a large number of brain volumes to be imaged, such as those using diffusion MRI or functional MRI.

3.5 On ghosts and pile-ups

Magnetic resonance images are susceptible to various different types of artefacts, which adversely affect their qualitative and quantitative interpretability and therefore need to be avoided or corrected for whenever possible (see for example Pusey *et al.*, 1986). We describe here the three most significant artefacts for diffusion MRI.

Firstly, there is the problem that the subject, which is usually a living and unsedated human patient or volunteer, may move during the scan. Even if there is no wholesale movement of the head, localised movement can occur as the subject swallows or moves his eyes. The ventricles, which are full of cerebrospinal fluid, typically exhibit spontaneous pulsatile movement; and dilation and contraction of the carotid arteries during the cardiac cycle can also be a source of this kind of artefact. The effect of motion during the sequence is to shift the phase of the signal originating from a particular location, which causes blurring and ghosting—that is, the appearance of nonphysical objects, or of a physical object several times. Motion artefacts can be alleviated by using a sequence that acquires images very quickly—generally EPI—and by “gating” image acquisition so that each slice is collected at the same point in the cardiac cycle (Lanzer *et al.*, 1984).

Whilst EPI is less sensitive to motion effects than other imaging sequences, it is considerably more vulnerable than other methods to two other types of artefact: eddy current induced distortions and susceptibility effects. We will describe these separately.

Eddy currents are tiny circulating electric current loops which are induced by the applied gradient fields, particularly when they are large in magnitude or switched rapidly. These in turn act as electromagnets with magnetic fields that oppose the effect of the gradient field, causing magnification, translation and shearing in the phase encoded direction of the image. The gradients used for diffusion imaging are particularly prone to produce this kind of artefact. One way to significantly reduce their effects is to use a twice-refocussed spin-echo sequence, as described by Reese *et al.* (2003).

Susceptibility effects occur at boundaries between materials with significantly different magnetic susceptibilities—as defined by Eq. (3.14). In the brain this is most obvious near di-

^cThis is the most common arrangement, but it is possible to use phase encoding in two dimensions, in which case selective excitation is unnecessary.

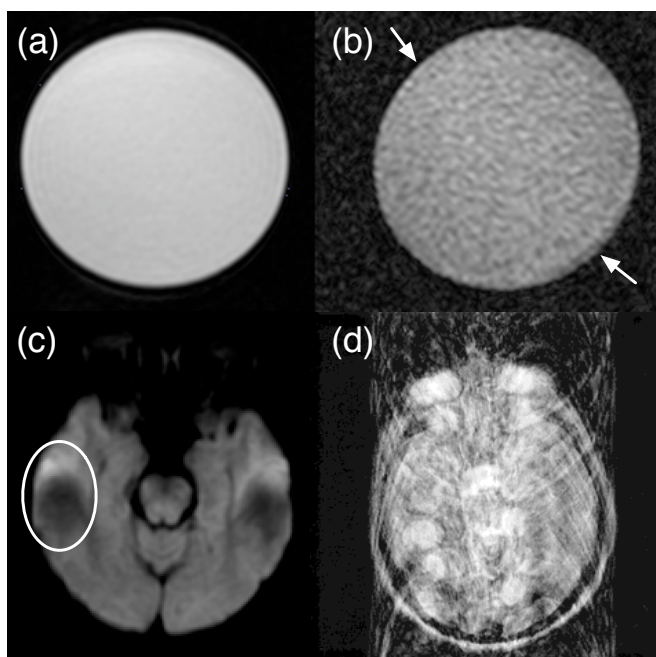


Figure 3.6: Examples of various types of MRI artefact. Eddy currents induce a distortion in (b) which results in this circular “phantom” appearing squashed relative to a reference image (a). (Note that the increased noise level in subfigure (b) is not caused by eddy currents.) A susceptibility effect near the ear canals produces signal pile-up and drop-out (c), resulting in artefactual bright and dark patches in the image. Motion by the subject can produce major blurring and ghosting effects (d). Subfigures (a–c) are courtesy of Dr Susana Muñoz Maniega; subfigure (d) is reproduced from Pipe (1999).

viding lines between soft tissue and air—around the sinuses, for example. At such boundaries, the field is locally distorted and therefore rendered inhomogeneous; and as a result signal can “drop out” of some areas while “piling up” in others. Strong susceptibility effects can also be seen if a subject has a small piece of metal near her head, like a hair clip.

Fig. 3.6 illustrates the effects of these different types of artefact. Image (b), which illustrates the distorting effect of eddy currents, is a diffusion-weighted image—as we will see in chapter 4, these images are particularly vulnerable to this sort of artefact. Image (d) is an extreme example of a motion artefact, which makes this image totally unusable.

Whilst not strictly an artefact, there is a further imaging issue which is important when it comes to interpreting MRI data. In practice, the FID is not retained in its original, continuous form, but rather sampled at regular intervals by an analogue-to-digital convertor. As a result the signal in the final image is discretised into spatial units with a fixed volume called **voxels**.^d The larger the dimensions of these voxels, the higher the signal to noise ratio of the image; but at boundaries between tissue types, the inhomogeneous signal will be averaged across the region represented by the voxel. This implicit averaging is called a **partial volume** effect. These effects make images hard to interpret, since one cannot easily tell what contribution white and grey matter, or healthy and unhealthy tissue, had to the measured signal value.

3.6 Summary

Beginning with a single proton, we have described in this chapter how the stochastic behaviour of atomic nuclei can be usefully represented at the macroscopic scale in terms of magnetisation. We have also demonstrated how this phenomenon may be manipulated using radiofrequency radiation, and then measured during relaxation to elucidate characteristics of living tissue. These techniques usually culminate, for clinical purposes, in the creation of images, whose formation we have also discussed. Finally, we have seen that the quality of magnetic resonance images can be affected by a number of artefacts, which arise as side-effects of the scanning process. It should be emphasised that MRI pulse sequence design, and artefact avoidance and correction, are both substantial fields in their own right; and many problems and solutions exist which have not been touched upon at all in the brief coverage of the last two sections.

In the following chapter we will focus on the specific application of the NMR effect to the measurement of diffusion.

^dThe word “voxel” is short for “volume element”, by analogy with “pixel”, which abbreviates “picture element”.